Seismic profiling of faults related to the 1886 Charleston, South Carolina earthquake: A collaborative US Geological Survey proposal

Project Award Number: # G17AP00040

Award Dates: February 2017 through May 2018

Submission date: August 31, 2018

Project dates: February 15, 2017 through May 30, 2018

Lee M. Liberty

Department of Geosciences

Boise State University

Boise, Idaho 83725-1536

Phone: 208-426-1419

lliberty@boisestate.edu

http://cgiss.boisestate.edu/~lml

Research supported by the U.S. Geological Survey (USGS), Department of the Interior, under USGS award number G17AP00040. The views and conclusions contained in this document are those of the authors and not be interpreted as necessarily representing the official policies, either expressed or implied, of the U.S. Government.

Contents

Abstract

We acquired 14 km of new seismic data over five field days in April, 2018 along the rural city streets and a CSX railroad access road in the vicinity of the southern isoseismal region of the 1886 earthquake to identify and characterize active faults. We identify a 4 km wide faulted and folded region along the CSX profile that is centered on the southern isoseismal zone of Dutton (1889). Additionally, we identify faults consistent with Quaternary motion on the Woodstock fault and within a N60E deformation zone identified by the studies of Chapman and Beale (2006) and Pratt et al (in prep). We identify slow shear wave velocities in the upper 10-20 m with increases in Vs that are consistent with the thickness of late Quaternary deposits. Ongoing analyses of these data will produce a Vs map for each profile and a comparison to high frequency site response estimates and liquefaction susceptibility.

Introduction

The 1886 Mw 6.9 to 7.3 Charleston earthquake was the largest earthquake in eastern U.S. recorded history (Bollinger, 1977; Bakun and Hopper, 2004) where nearly every building in the Charleston area was damaged or destroyed. Widespread liquefaction throughout the epicentral region was documented (Dutton, 1889; Figure 1) and more than 100 people were killed (Bollinger, 1977). A similar earthquake today would be devastating to the region (Wong et al. 2005). The earthquake was centered about 20 to 30 km west and northwest of Charleston, where a northeast-trending isoseismal pattern was documented (Dutton, 1889; Figure 1). The faults that caused the 1886 earthquake remain unknown because no surface scarps are identified and the modern seismicity forms a cluster without clearly delineated faults (e.g., Chapman et al., 2016; Figure 1). To date, the mechanism to identify faulting is through seismicity, reflection seismology, and geomorphic alignments, but these data are sparse. Although paleoliquefaction features indicate strong shaking every 500 to 600 years in southeast South Carolina (Talwani and Schaefer, 2001), the recurrence times for specific faults remain unknown. Thus, high resolution studies are needed to further constrain fault locations and kinematics to better assess earthquake hazards.

Figure 1 shows a summary of mapped faults in the study area. Because there is no surface expression of these faults and because there is limited subsurface coverage, the locations, geometries and fault lengths are poorly constrained. This data paucity has resulted in many fault interpretations. From topography and stream gradients, Marple and Talwani (1993 and 2000) mapped the East Coast fault to extend through Ravenel and Summerville regions. This fault is consistent with 1) a region of modern seismicity termed the Middleton Place-Summerville Seismic Zone (Dura-Gomez and Talwani, 2009; Chapman et al., 2016), 2) within the 1886 epicentral region (Figure 1; Dutton, 1889), 3) an inflection in reflectors along profile VT2, and 4) offset strata identified on COCORP C-2 profile (Chapman and Beales, 2006) and USC-5 profile (Marple and Miller, 2006). Subsequent interpretations by Talwani and Katuna (2004) and Talwani and Dura-Gomez (2009) revised the fault geometry and locations based on a new catalog of seismicity and structural models. They termed the right-lateral strike slip Woodstock fault as the dominant structural fault in the region, but sparse mapping and low resolution seismic limits fault characteristics.

Previous seismic reflection campaigns in the epicentral region of the Charleston earthquake (Figure 1) include four seismic reflection profiles (C1–C4) acquired by the Consortium for Continental Reflection Profiling (COCORP) in the Summerville area (Schilt et al., 1983). Virginia Tech also acquired relatively deep seismic reflection profiles (VT1-VT5) in the same region during a similar time (Coruh et al., 1981). The US Geological Survey collected profiles SC1–SC10 (Hamilton et al., 1983) and the Kansas Geological Survey collected five additional seismic profiles (USC1-USC5) (Marple and Miller, 2006). Finally, Buckner (2011) reprocessed a long industry seismic reflection profile in the area (SEISDATA4) that extended through the southern isoseismal area. Many of the university and USGS profiles were reprocessed by Chapman and Beale (2010) to show an early Mesozoic extensional basin with compressional reactivation of Mesozoic extensional faults. Subtle reflector inflections best point to presumably active faults within the Middleton Place-Summerville Seismic Zone and within the broader 1886 epicentral zone. These offset reflectors are best seen along the eastern portion of COCORP profile C-2 (Chapman and Beale, 2010).

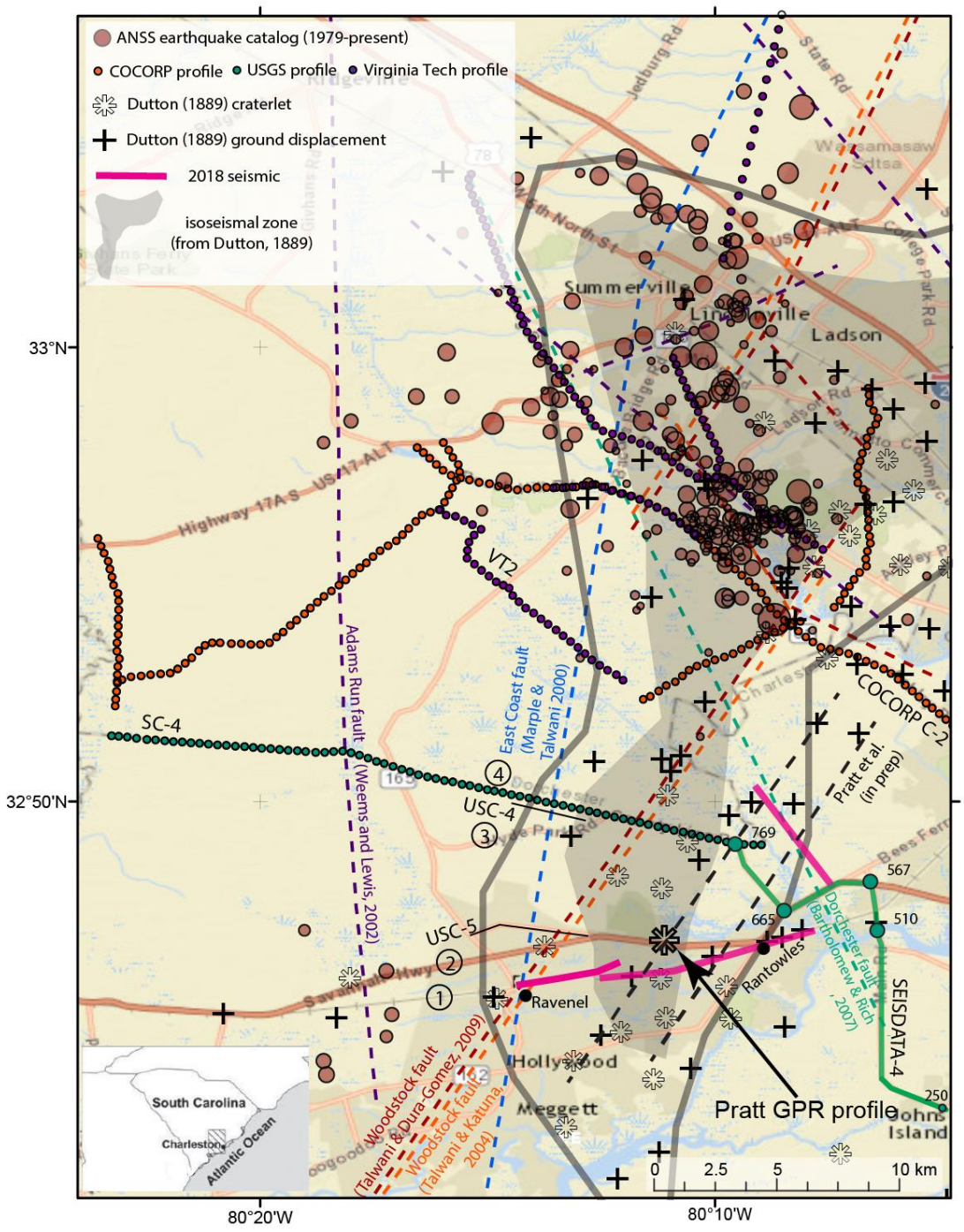

Figure 1. Map of the study area with the mapped faults (dashed), horizontal displacement and craterlet regions (plus and asterisks) from Dutton (1889), ANSS earthquake epicenters (red circles) isoseismal zones from 1886, and the location of previous seismic surveys (from Chapman and Beale, 2006; Marple and Miller, 2006). Seismic profiles acquired as part of this study (pink lines) lie within the southern isoseismal/deformation zone where little subsurface information is currently available. Note the NE alignment of streams and 1886 craterlets and ground displacements that may point to unmapped faults.

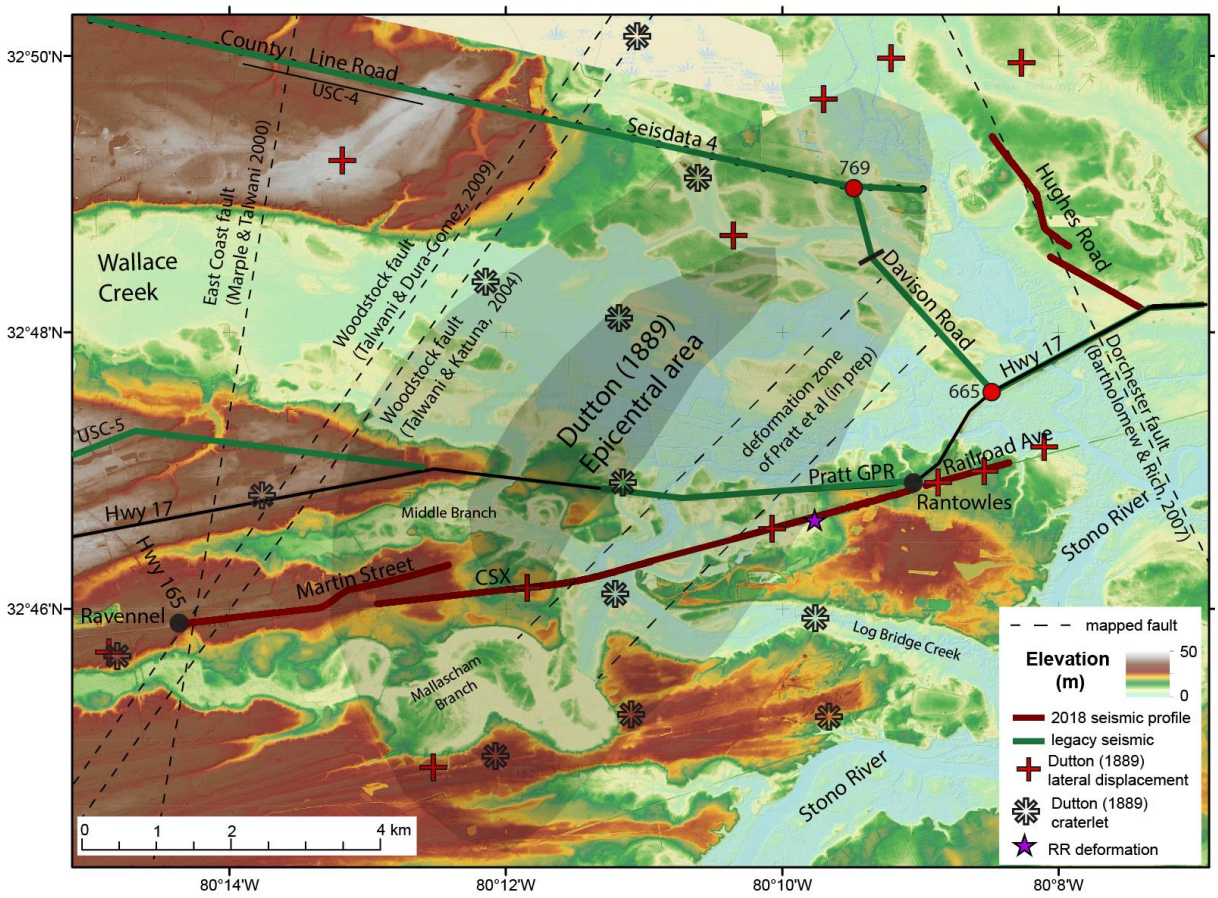

Figure 2. Study area topographic map with highways and waterways that support this report. Additional annotations include isoseismals (gray ellipses) related to the 1886 southern epicentral area of Dutton (1889), legacy (green) and new (red) seismic profiles, mapped craterlets and lateral displacements from 1886 (Dutton, 1889; Heidari, 2011), and mapped faults from previous studies (dashed lines).

Whereas many of these seismic profiles extend through the Summerville area, few profiles have focused on the southern region that experienced significant damage and liquefaction in 1886 (Figure 1). Offset reflectors on profiles C2 and USC-5 are consistent with the Talwani and Dura-Gomez (2009) interpretation of the Woodstock fault, but reflector geometries on these and other seismic profiles point to a number of additional faults that cut through the 1886 epicentral region (Figure 1). Only seismic profile SC-4 and SEISDATA4 crossed the southern epicentral zone that contains extensive ground displacements and liquefaction (craterlet) features documented in 1886 (Figure 1). The most pronounced structure (diffraction and anticline) lies at the very eastern end of the SC-4 profile near the intersection of County Line Road and Davison Road (Figure 2) where craterlets and ground displacements from 1886 were observed (Chapman and Beale, 2010; Figure 2). Buckner (2011) identified offset reflectors farther west, where Talwani and Katuna (2004) and Talwani and Dura-Gomez (2009) interpreted the Woodstock fault (Figure 2). Many more surface displacements are noted by Dutton (1889) and Heidari (2012) farther east than the SC-4 profile. Although subtle reflector offsets are identified on many seismic profiles, the low resolution and lack of shallow coverage of these data limit interpretations.

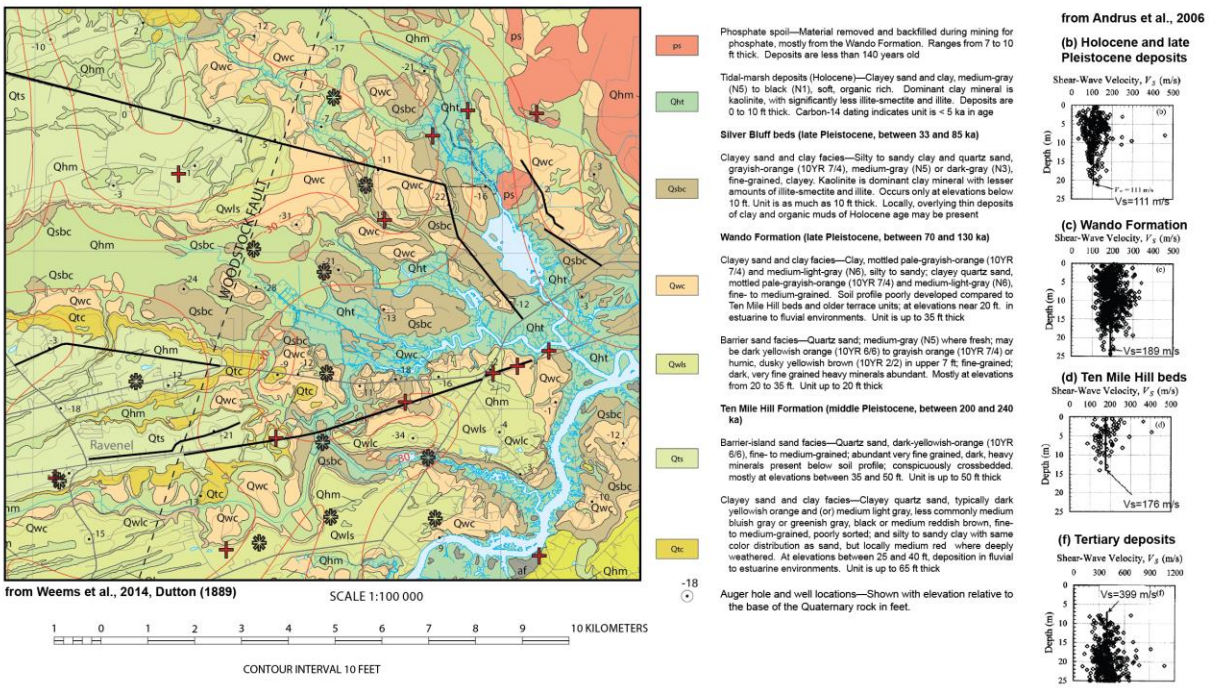

Figure 3. Geologic map from Weems et al. (2014) along with new and legacy seismic profile locations (black lines). Geologic units near seismic transects are described in legend. Lateral displacements and craterlets of Dutton (1889) are shown (from Figure 1). Vs measurements from Andrus et al (2006) are shown for each unit.

Recently, the USGS (T. Pratt) reevaluated existing seismic reflection, magnetic, and geomorphic data and acquired new ground penetrating radar (GPR) profiles in the vicinity of liquefaction craterlets and surface ground displacements near Rantowles (Figure 2). The GPR data show reflectivity to 15+ m depth and Pratt identified at least one intriguing stratigraphic offset in the study area that suggests a meter step down to the west at the base of Quaternary strata (Figure 2). F. Pazzaglia (personal comm.) has identified some anomalous river meanders in this region that, when combined with new GPR data, may suggest a more northeast-trend when compared to the mapped Woodstock fault trace (Figure 1). The focus of this study is to present new high resolution seismic data in this region to identify offset reflectors that may indicate active faults.

Previous liquefaction and site response studies

Liquefaction was widespread throughout the 1886 epicentral area (Figure 1 and 2). Chapman et al. (2006) noted that the shallow impedance contrast between low velocity (100-200 m/s) Quaternary sediments and the underlying higher velocity (300-600 m/s) Tertiary rock largely controls the 1-10 Hz earthquake site response and the Quaternary layer thickness is the most important parameter to characterize site response and liquefaction susceptibility for the Charleston area. Within this frequency range, site response can vary by a factor of three, where Tertiary rock depth can be as shallow as a few meters. Andrus et al (2006) and Heidari and Andrus (2012) updated focused on variations in shear wave velocities to show beach sand, estuarine and fluvial surficial deposits are present at the 1886 ground displacement and craterlet sites (Figure 3), with the Ten Mile Hill formation correlated with the greatest instances of liquefaction. Because the dominant earthquake response lies within the frequency band of active

sources, and both site response and liquefaction effects are tied to shallow shear wave velocities and water depth, we explore examine both shear wave (Vs) and p-wave (Vp) velocity maps.

Seismic approach

Land streamer technology has gained support and use for the past 15 years. Van der Veen and Green (1998) first constructed and tested land streamers with gimbaled geophones. Their interest was in rapid Vp reflection acquisition, but recognized the potential to integrate a variety of seismic source and receivers into this technology. For the past decade, other land streamer designs have been developed and integrated with hammer, weight drop, and vibroseis sources. Boise State land streamers were first developed with EHP funds (#G13AP00032) to develop 1-, 2- and 3-component systems. Integrated with accelerated hammer sources and GPS positioning information, we can simultaneously record body wave and surface wave signals to obtain detailed images beneath urbanized regions (Figure 4).

We acquired approximately 14 km of seismic data over five field days during April, 2018 along the rural city streets and a CSX railroad access road (Figure 2) in the vicinity of the southern isoseismal region of the 1886 earthquake (Dutton, 1889; Figure 2). The new seismic data were collected at a nominal 2.5 m shot spacing using a 50 kg hitch-mounted accelerated weight drop source and 72 vertical-component, 10 Hz baseplate-coupled geophones spaced at 1.25 m, embedded in fire hose (Liberty and Gribler, 2014). The weight drop source operates directly on city streets during business hours with no resulting road surface damage (Liberty, 2011). A single operator controls the source, recording system, and streamer positioning. The source produces broad band impulsive signals between about 5-300 Hz. We pulled our seismic streamer at a distance of 5 m behind the seismic source. Thus, we collected more than 5,300 72-channel shot gathers with a 90 m receiver aperture. Timing between shots (single hammer hit per location) was approximately 15 s, resulting in about 480 m/hour rate of data acquisition. Rain delayed our operations for much of one day.

We extract first arrivals to obtain p-wave (Vp) seismic measurements to 20-30 m depth, Rayleigh wave dispersion curves to obtain shear wave (Vs) seismic profiles to about 25 m depth, and reflection signals to map subsurface horizons to 300-500 meters below land surface. We utilize a differential GPS system to obtain accurate position measurements during data collection with a decimeter-precision odometer mounted to the source vehicle to provide accurate source positioning. We then use DEM derived elevations (https://viewer.nationalmap.gov/) for subsequent seismic processing where dense tree cover precluded robust elevation measurements. Distances along each profile are with respect to the first source position. Some seismic profiles were obtained with the assistance of a certified road survey crew to control traffic both along city streets and along the CSX rail access road.

Seismic properties

For unconsolidated sediments, seismic velocities are strongly controlled by lithology, fluid content and porosity (e.g., Mavko et al., 2009). The largest Vp contrast that we encounter is found at the transition from dry to saturated unconsolidated sediments and at the transition from unconsolidated Quaternary strata to consolidated Tertiary and older strata. Where saturated unconsolidated sediments are found, we typically observe seismic velocities that exceed the speed of sound in water (about 1,500 m/s), with the average velocity for saturated coastal plain

sediments at about 1,800-2,000 m/s (e.g., Chapman and Beale, 2010; Buckner, 2011). Within the vadose zone, Vp typically ranges from between 350-1400 m/s. The depth to water saturation (http://www.dnr.sc.gov/water/hydro/WellRecords/locatewells) and the depth to Tertiary strata (e.g., Weems et al., 1987) both lie within the upper ~10-30 m below land surface, thus refraction tomography may not adequately separate lithology changes from saturation effects within these depth ranges.

Vs is strongly tied to soil and rock stiffness and less dependent on fluid saturation when compared to Vp (Boore and Atkinson, 2008; Mavko et al., 2009). In the Charleston area, Vs in the upper 30 m range from about 100-700 m/s, with the slower velocities typically found beneath the lower elevation regions where Holocene/Pleistocene deposits are mapped (e.g., Andrus et al., 2006; Weems et al., 2014). Vs for Tertiary strata generally lie above 300 m/s (Andrus et al., 2006). Given the larger contrast between Pleistocene and Tertiary strata for Vs compared to Vp, both above and below water table depths, we utilize Vs to map the depth to Tertiary strata that strongly influences high frequency site response. This analysis is presented for select profiles and analysis is continuing beyond the timeline of this report.

Vp derived from head waves

On select profiles, we identify the first arrival time as the first ground motion for each source/receiver pair (Figure 4). First arrivals were picked both from unprocessed field records and filtered field records in both shot and offset domains. Given the large seismic energy source with respect to limited receiver offsets, first arrivals on an asphalt/gravel road surface were typically clean and easy to pick in the presence of traffic noise (Figure 4). Vp values in about the upper 2-3 meters are poorly constrained due restricted geophone offsets.

We use a travel-time tomography code to estimate the shallow velocity structure (modified from St. Clair, 2015). The velocity model is parameterized as a mesh of constant velocity cells with a fixed horizontal width and a vertical thickness that increases with depth. The strategy is to generate a reasonable starting model and then alternate between: 1) shortest path ray-tracing (Moser, 1991) to predict travel-times for the current model and 2) using a linearized inversion with smoothness constraints to map the residual travel-times (predicted – observed) into an updated model with a smaller root mean squared (RMS) misfit (e.g., Zelt et al., 2013). The process is terminated when RMS misfit between successive iterations becomes negligible.

Quantifying model uncertainty and resolution of tomographic models is a difficult task because of the large number of models that need to be tested. Uncertainty tests that explore the relationship between starting models and final solutions can show standard deviations upwards of 25% for individual model parameters. Higher values (>15-20%) typically correspond to regions with strong velocity gradients or low ray coverage, but similar results are observed when comparing results from different algorithms (Zelt et al., 2013). Even in the presence of these uncertainties, large scale features such as depth to bedrock and strong lateral velocity changes tend to be well resolved using any refraction analysis approach.

Vs derived from Rayleigh waves

On select profiles, the Rayleigh wave signals were extracted and processed via the multichannel analysis of surface wave (MASW) approach (Park et al., 1999) using both Kansas Geological Survey Surfseis software (http://www.kgs.ku.edu/software/surfseis/) and in-house Matlab code for picking dispersion data (Gribler et al., 2016). The Rayleigh wave signals provide estimates of

subsurface elastic (stiffness) conditions where rapid data collection is possible without compromising results when compared directly measuring shear wave velocities through head wave or downhole measurements (e.g., Stephenson et al., 2005).

Frequency-phase velocity dispersion plots were generated for each (2.5 m spaced) shot gather and peak semblance picks from these plots were inverted to generate Vs profiles for the upper 20-30 m (Figure 4). Rayleigh wave frequencies that are recorded with the land streamer system typically range from 3-60 Hz (e.g., Gribler et al., 2016). Once Vs profiles were calculated, 1-D velocities were combined to obtain 2-D Vs profiles with depth. Vs30 values were then calculated for each receiver spread midpoint location (e.g., Boore et al. 1993), averaging and smoothing values over 50 m.

We adopt the NEHRP soil classification to describe Vs (IBCO, 2000). Here, we describe E-class (less than 180 m/s) as soft soil; D-class between 180-360 m/s as stiff soil; C-class between 360-760 m/s as dense soil or soft rock; and B-class above 760 m/s as rock, locally correlated with Tertiary strata. For display, we use NEHRP sub-classifications of Wills et al (2000).

For each seismic profile, we compute a frequency plot for each gather (Figure 4). We obtain signals from recorded offsets beyond 30 m (to remove near source effects) and then sum these signals along each profile to obtain the dominant (surface wave-derived) frequency (to as low as our source can provide). Because Chapman et al. (2006) noted that a 1-10 Hz earthquake site response is controlled by shallow impedance contrasts, we compare our surface wave frequencies to calculated Vs and mapped lithology. Ongoing studies using a grid search approach to identify the depth to Tertiary strata will be completed this fall and presented at a national meeting and included in a journal article.

Reflection profiling

Because surface waves tend to dominate the recording systems dynamic range at near offsets, we extract coherent reflections between first arrival head waves and Rayleigh wave signals for reflection processing (Figure 4). This reflection window has been termed the “optimum window” (Hunter et al., 1984) and for shallow, limited aperture seismic surveys, this window contains reflection signals that are not contaminated with surface waves. In the presence of saturated unconsolidated/semiconsolidated sediments, the optimum window allows robust velocity analyses for the upper ~500 m depth.

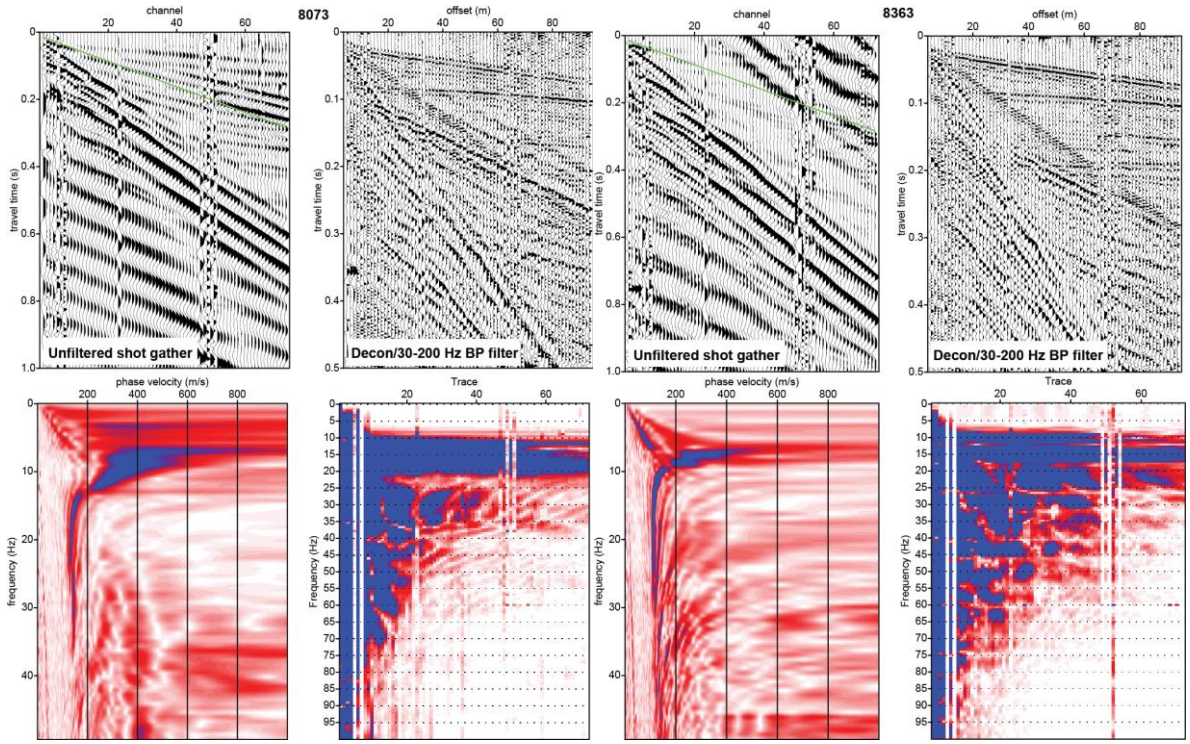

Figure 4. (top) Unprocessed and deconvolved/filtered shot gathers from Railroad Avenue showing both surface waves and reflections. The green line on the unfiltered gather represents air wave velocity of 330 m/s. (Bottom) Dispersion and frequency plots for (top) gathers showing surface wave signals below 10 Hz. We sum the frequency panel along each profile to discuss changes in dominant frequency along each profile.

We processed the data using Halliburton's ProMAX® seismic processing software with a standard processing approach outlined by Yilmaz (2001). Geometry was applied to each source and receiver location from differentially corrected GPS positions recorded each shot record and via DEM-derived elevation values. Processing steps included datum statics, spiking deconvolution, bandpass filter, surface wave attenuation through a two-step singular value decomposition approach to estimate and adaptively subtract the ground roll signal, iterative velocity analyses with dip moveout corrections, amplitude gains, and a post-stack time to depth corrections. Post-stack migration is selectively applied to the data, but migration artifacts can distort key reflector geometries and are used selectively. Where surface waves dominate the gathers and signal processing steps, bottom mutes were applied to remove this signal and improve stacked reflection results. Depths were estimated using 1-D averaged stacking velocity models. Water well (http://www.dnr.sc.gov/water/hydro/WellRecords/locatewells) and engineering borehole logs (Weems et al., 1987) help constrain lithology and depth to water table for interpretation.

Seismic results

Railroad Avenue

The one km long west to east Railroad Avenue seismic profile extends from Hwy 162 at Rantowles to the eastern road termination at a foot bridge near Wallace Creek (Figure 2). The profile parallels the CSX rail line to the north along a residential dirt road and the road surface contains a gentle 5 m decrease in elevation from west to east (Figure 5). Weems et al. (2014) mapped late Pleistocene Wando Formation sands along the western 2/3 of the profile and clays along the eastern 1/3 of the profile (Figure 3). An auger hole (RA-16) near the western limits of the profile places the Tertiary Ashley formation at 6.7 m depth (Weems et al., 1987). The water table is noted at about 8 m depth in nearby water wells. Dutton (1889) identified two lateral displacement features from the 1886 earthquake, adjacent to the rail line (locations obtained from Heidari, 2011).

First arrival picks from 432 shots were clean to all recorded offsets, allowing Vp measurements for the upper 20-30 m depth. Rayleigh wave dispersion was picked between about 10-40 Hz, allowing Vs estimates to 20-25 m depth. Reflections were observed to about 0.4 s two-way travel time, or about 0.4 km depth.

Vp for the upper few meters ranges from 500-700 m/s (Figure 5). The Vp gradient is consistent across the profile, and the 1,500 m/s contour is measured between 7-9 m depth along the profile. We assume the 1,500 m/s contour represents the depth to water saturated sediments, consistent with water well measurements. The depth top of Tertiary strata is not clearly differentiated from the depth to water saturated sediments due to comparable increases in Vp at comparable depths for these two boundaries. We measure an average Vs of 170 m/s for the upper 5 m depth, consistent with Vs averages for the Wando Formation (Andrus et al., 2006 measurements average 189 m/s; Figure 3). We measure an average Vs between 10-20 m depth of 418 m/s for the underlying Tertiary strata (Andrus et al., 2006 measurements average 399 m/s; Figure 3). Vs20 variations along the profile range from 250-350 m/s with higher values at the lower elevation eastern portion of the profile. We tie NEHRP Class E soils (<180 m/s) to Wando Formation strata and NEHRP Class C and D soils (>180 m/s) to Tertiary strata, consistent with a decrease in Wando Formation strata along the eastern portions of the profile. The slowest Vs20 values are consistent with the location of lateral displacement zones of Dutton (1889), suggesting that these slower Vs zones may have produced permanent deformation during the 1886 earthquake. The frequency-distance plot (Figure 5d) shows the dominant source response varies from 9-12 Hz.

Seismic reflection results (Figure 5) show strong amplitude flat lying continuous reflectors in the upper few hundred meters, suggesting no measurable faults are located along this profile within Tertiary or older strata.

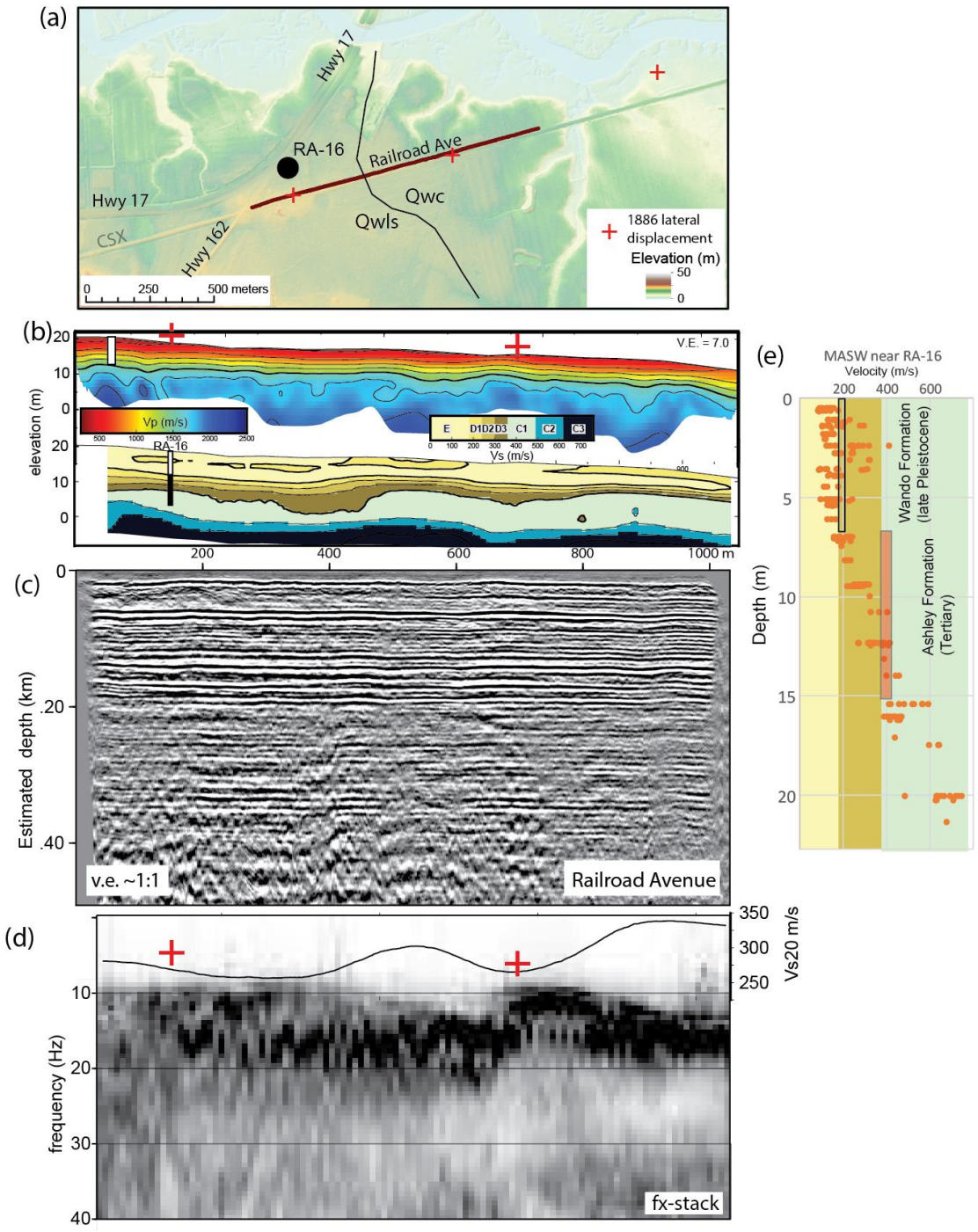

Figure 5. (a) DEM showing profile location near the intersection of Hwy 162 and Hwy 17 near Rantowles; (b) Vp and Vs profiles with depth to water table and Tertiary strata; (c) Seismic reflection profile; (d) Vs20 and fx stack showing Vs/frequency relationship; (e) Vs with depth for the western shots, compared to RA-16 auger results and velocity averages(rectangles) from Andrus et al (2006).

CSX railroad

The 6.55 km west to east CSX profile extends from Salters Hill Road to Hwy 162, immediately west of Rantowles, SC (Figure 2). The western portion of the profile overlaps with the Martin Street profile, and the profile continues to the east along Railroad Avenue to provide a continuous transect from Ravenel to Rantowles. Weems et al. (2014) mapped Pleistocene sands and clays of the Wando and Ten Mile Hill formation on elevations that range from 0-30 m above sea level (Figure 6). The Ten Mile Hill formation is mapped mostly along the western half of the profile and the Wando Formation is mapped mostly along the eastern half of the profile, separated by the Mallascham Branch of Wallace Creek. From auger data, Weems et al (1987) estimated the depth to Tertiary strata at less than 10 m along the length of the profile. Weems et al. (2014) mapped the northeast-trending Woodstock fault immediately to the west of this profile, Pratt et al (in prep) mapped a northeast-trending deformation zone across the center of this profile, and Chapman and Beale (2010) identified two northeast-trending deformation zones that project across this profile at about a N60E trend. Dutton (1889) characterized the central portion of this profile as in the southern epicentral region of the 1886 earthquake (Figure 2), and identified lateral displacement and craterlets along the rail line (Figure 6). Seismic data show reflectivity to about 0.5 km depth. Seismic refraction (Vp) and surface wave (Vs) analyses are currently underway for this profile.

Seismic reflection results, migrated and depth converted, show a broad symmetric syncline centered near position 3.5 km, beneath the Mallascham Branch of Wallace Creek (Figure 6). This fold shows about 50 m change in elevation on the 100-300 m deep reflectors. Although we do not identify significant stratigraphic offsets, we define faults that separate km-wide zones of differential stratigraphic dips within the synclinal fold. From reflector dips, we identify faults that dip from 45-90 degrees, consistent with a 4 km wide zone of long-lived deformation. These faults project to the surface where Dutton (1886) identified surface deformation related to the 1886 earthquake (Figure 1).

On figure 6, we show the fx-stack that highlights the dominant surface wave frequencies along the profile. To the east of the Mallascham Branch where Wando Formation strata are mapped, we observe a dominant seismic frequency of 6-10 Hz. To the west of the stream, we observe two dominant frequencies that likely represent fundamental and higher mode surface wave signals. A large contrast in dominant frequency is noted at the eastern margin of the stream channel. This change in dominant frequency is coincident with mapped craterlets that resulted from the 1886 earthquake. We are currently exploring this changing signal with surface wave modeling to extract shear wave estimates with depth.

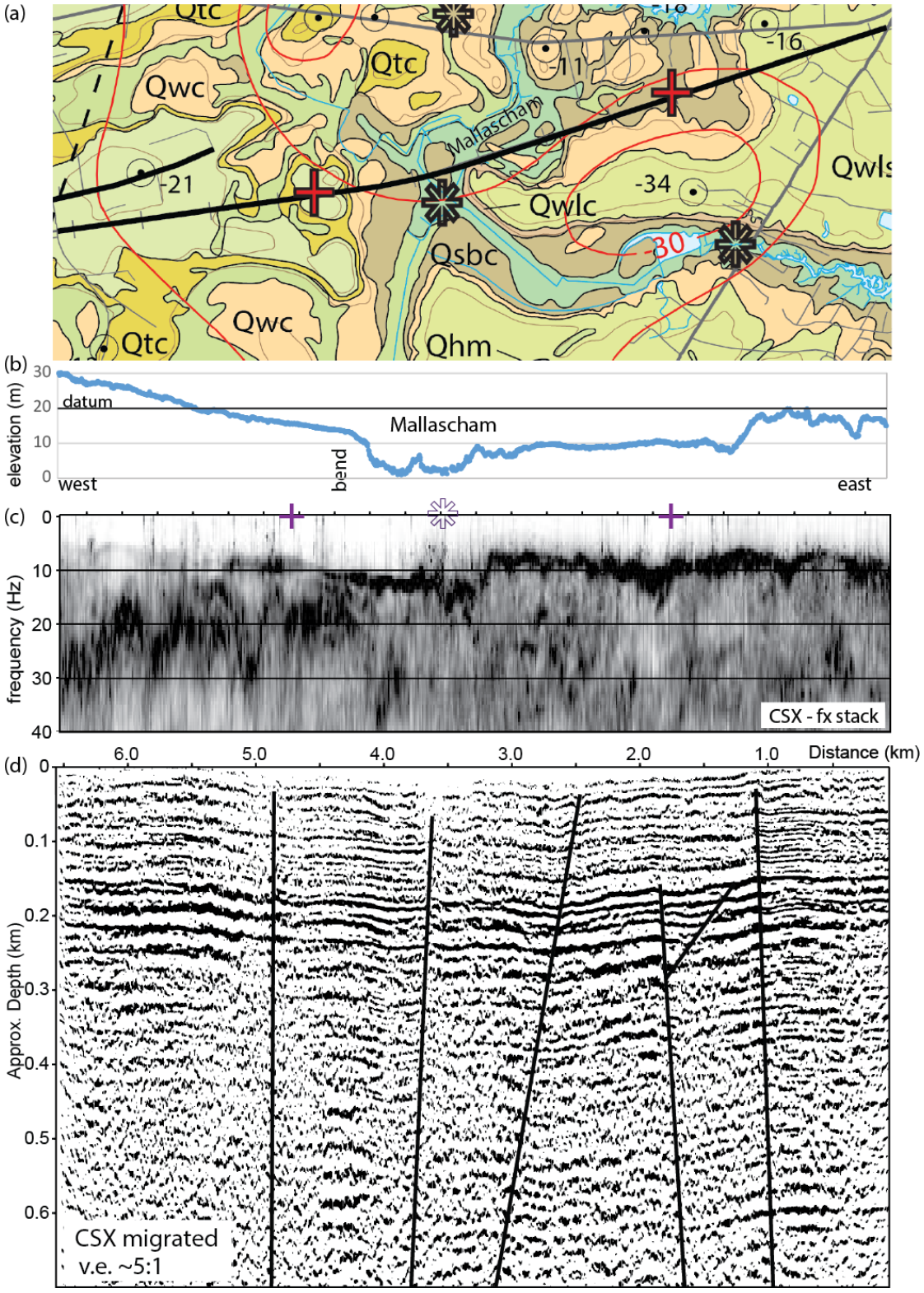

Figure 6. (a) Geologic map of Weems et al (2014) for the CSX profile. Craterlets and lateral displacements of Dutton (1889) are noted along the profile. (b) elevation profile for the CSX profile. (c) fx stack for the CSX profile. (d) reflection stack and interpreted faults for the CSX profile. Faults are mapped at reflector truncations and changing reflector dips.

Martin Street

The 3.15 km west to east Martin Street profile begins immediately east of the Ravenel rail station and terminates at the end of road (Figure 2). The eastern portion of the profile overlaps (in longitude) with the CSX profile to provide a continuous transect from Ravenel to Rantowles. Weems et al. (2014) mapped Pleistocene sands of the Ten Mile Hill formation on elevations that range from 25-35 m above sea level (Figure 3). Mapped strands of the northeast-trending Woodstock fault cross the western portion of the profile (Talwani and Katuna, 2004; Talwani and Dura-Gomez, 2009; Weems et al., 2014) that was identified on legacy seismic profile USC-5 (Marple and Miller, 2006), approximately 2 km to the north. Dutton (1889) did not identify lateral displacement or craterlets along this profile (Figure 2).

Figure 7 shows the refraction results and migrated depth converted stack for Martin Street. Vp derived from refraction results show water saturation at about the 1250 m/s contour (http://www.dnr.sc.gov/water/hydro/WellRecords/locatewells), consistent with partially saturated clays that are logged in a nearby auger hole (RA-3; Weems et al., 1987). This velocity contour also is coincident with a high ray density zone identified from bending rays at this velocity boundary. Two auger holes note the transition from Pleistocene to Tertiary strata at about 15 m depth, consistent with the 1,550 m/s Vp contour. The undulating contours below water table depths may represent changes in lithology or saturation along the profile, but ray coverage diminishes below the water table. Vs mapping from surface waves is currently underway.

We observe high quality first arrivals and reflectivity to more than 0.3 km depth, with diminished reflection quality at greater depths. The reflectors dip slightly (less than one degree) to the east with a notable paleochannel at about .05 km depth between 0.1-1.5 km distance (Figure 7). We identify offset and tilted reflectors within a 100 m wide zone along the west side of the paleochannel that we interpret as faults (f1 and f2). We interpret an additional fault (f3) at about 2.5 km distance where we identify west dipping reflectors to the east of the fault. Faults f1 and f2 are close to the mapped location of the Woodstock fault (Figure 1 and 7), although we show a narrow deformation zone that contrasts the broad deformation zone of Marple and Miller (2006) along profile USC-5. Because we do not identify a similar fault to f3 along the CSX profile, we interpret a northeast fault trend, consistent to the regional structural trend of most published studies. Vs mapping for this profile is currently underway to assess site response for this region.

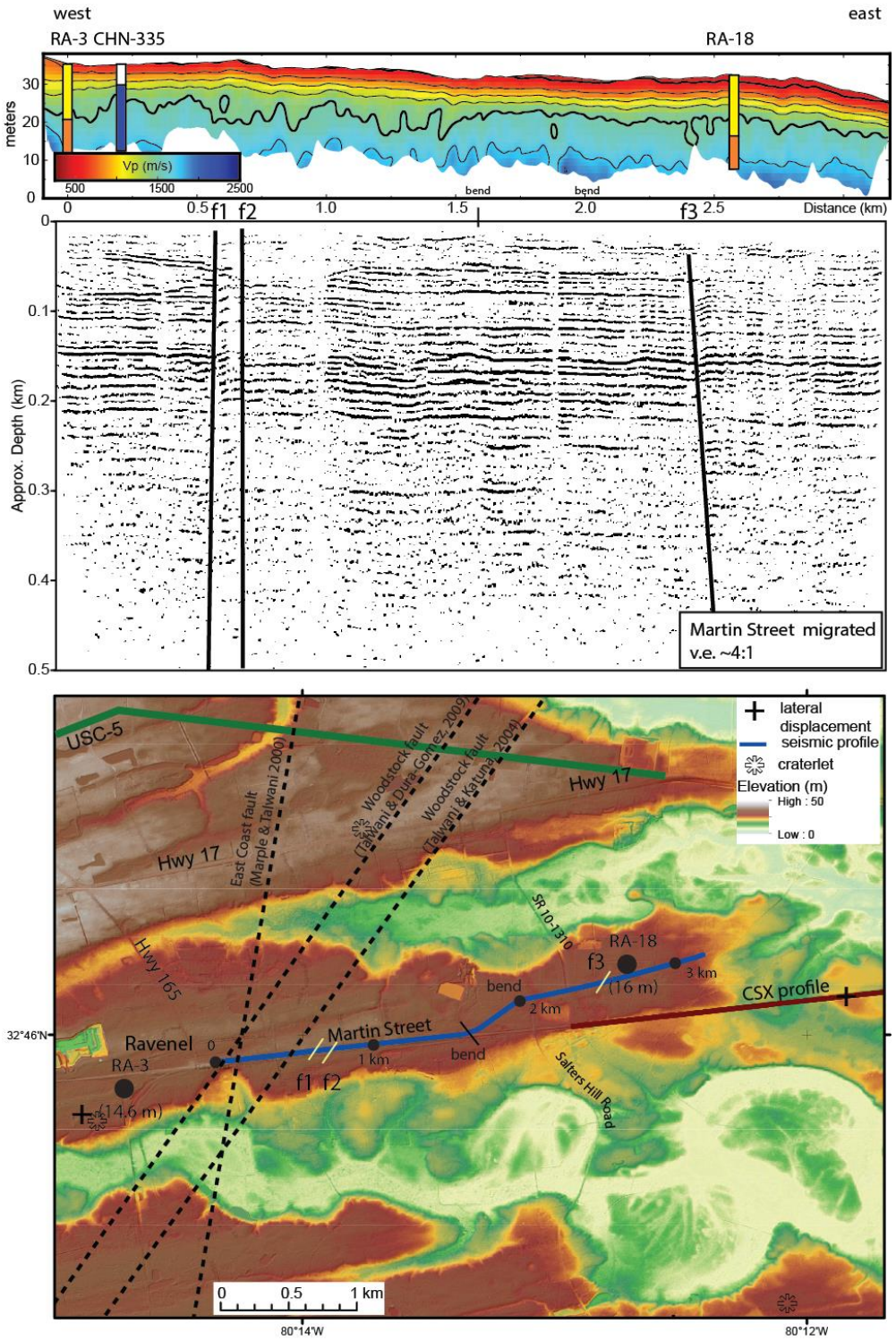

Figure 7. (top) Martin Street refraction and migrated/depth converted reflection profile. Note the reflector truncations/offsets where we identify faults. The faults at ~0.6 km are close to the Woodstock fault location from Talwani and Katuna (2004). (bottom) Topographic map with seismic profile location and mapped faults. Yellow hash marks represent seismically mapped faults.

Hughes Road

The 2.6 km northwest to southeast Hughes Road (state road 10-738) profile consists of two segments (Figures 2 and 8). The northern segment extends from the road termination at a private residence southeast to a bend in the road and along the length of Dawning Lane (Figure 8). The southern segment begins on a private driveway and extends to the southeast to the Hwy 17 intersection. Approximately 6 m of elevation change is observed along this profile. Weems et al. (2014) mapped Pleistocene clays and sands of the Wando formation along the length of the profile (Figure 3). Weems et al (1987) identified the depth to Ashley River Tertiary strata at 2.7 m depth at auger hole RA-20 (Figure 8). The north-trending Dorchester fault was mapped to cross this profile (Bartholomew and Rich, 2007), but no field evidence for this fault was provided near Hughes Road. Chapman and Beale (2010) connect a fault identified on seismic profiles SC4 and C2 to extend across this profile. Dutton (1889) did not identify lateral displacement or craterlets along this profile (Figure 2).

The migrated, depth converted stack shows mostly flat-lying reflectors to more than 0.6 km depth (Figure 8). A 0.3 km wide zone near 1 km distance shows a step down in lower amplitude reflectors. This pattern is consistent with faults that cross Hughes Street near the northern limits of the profile. The dominant frequency along the length of the profile ranges from 10-20 Hz. This frequency content is higher than that measured along the CSX (Figure 6) and Railroad (Figure 5) profile and is consistent with a thin layer of Quaternary sediments over Tertiary strata. Ongoing Vp and Vs analyses will relate shallow properties to the dominant surface wave frequency.

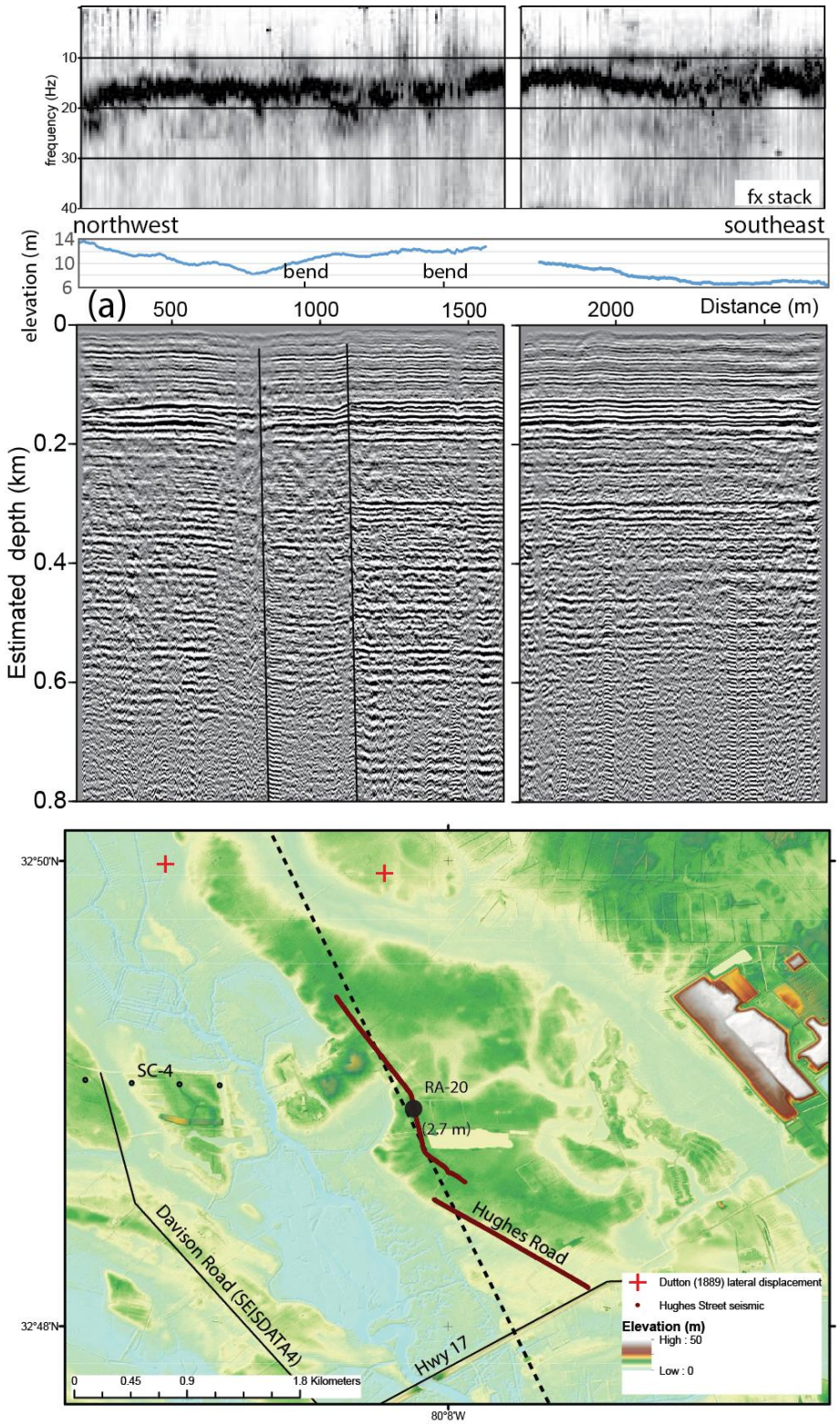

Figure 8. (top) FX stack for Hughes Road transect showing a dominant surface wave frequency of 10-20 Hz, higher than measurements along other profiles. (middle) migrated depth converted stack. (bottom) DEM for Hughes Road profile showing two seismic segments.

Discussion and Summary

Figure 9 shows the seismic profiles acquired as part of this study. Additionally, the Seisdata4 profile of Buckner, 2011 is presented to compare with our new seismic results. This profile extends along Davison Road between CSX and Hughes Road profiles. The most notable evidence for faulting related to the 1886 earthquake (and other Quaternary earthquakes) is located along the CSX profile of the Ravenel to Rantowles transect. Here, a 4 km wide synclinal fold contains reflector truncations and laterally changing dips that are consistent with faulting. This deformation zone lies within the maximum ground shaking (southern) isoseismal focus area of Dutton (1889). Reflection profiles to the west and east show mostly flat lying reflectors, but the Martin Street profile does show evidence to extend the Woodstock fault to as far south as Ravenel. A narrow fault zone is identified along the Hughes Road profile. Although the Seisdata4 profile does not image reflectors in the upper 0.2 km, we would expect to see deformation on deeper reflectors if the mapped CSX faults extend to the northeast at the N60E trend of regional mapped faults. This inconsistency may be due to 1) lateral changes in faulting where regions outside the isoseismal zone have consistently experienced less dip-slip motion or deformation, 2) the faults imaged on the CSX profile terminate to the southwest of Davison Road, or 3) the fault trend is not close to N60E. Seismic profile SC4, located along County road to the north of the CSX profile, do not show obvious folding or faulting, but this profile is also similar resolution as the Seisdata4 profile and does not contain reflectivity in the upper 0.2 km. The USC-5 profile of Marple and Miller (2006) shows a deformation zone similar in width when compared to our CSX results, but they did not observe a syncline within the deformation zone. To connect these two deformation zones would require a fault trend not observed in this region.

The syncline along the CSX profile is similar to the Chapman and Beale (2010) synclinal fold observed along profile C-2 to the northwest of this profile (Figure 1) and is similar to a syncline noted near CMP 570 at about 0.45 km depth on the Seisdata4 profile (Figure 8). However, the fold on C-3 was broader (>10 km) and was noted at about one km depth. The fold along the Seisdata4 profile is similar in dimensions, but is located too far east to relate to the CSX deformation zone. The easternmost portion of profile SC-4 parallels the CSX profile, extends farther east than the Seisdata4 profile, and Chapman and Beale (2010) noted that the best evidence for tectonic deformation would project between the C-2 and CSX profiles along the very eastern limits of SC-4, or a N60E trend. Additionally, the GPR profile of Pratt et al (in prep) places deformation along this same trend and stream channel orientations project this deformation to the central portion of the CSX profile. Thus, our seismic results support a NE-trending zone of faulting that decreases in amplitude to the northeast, consistent with the limits of the southern isoseismal zone of Dutton (1886).

Vs estimates from Rayleigh waves are consistent with the studies of Chapman et al (2006) and subsequent studies. We are currently modeling Vs distributions to relate to site response, liquefaction susceptibility, and paleoliquefaction. We show that Vs mapping is a more robust approach to estimating the thickness of late Quaternary strata when compared to Vp mapping via first arrivals.

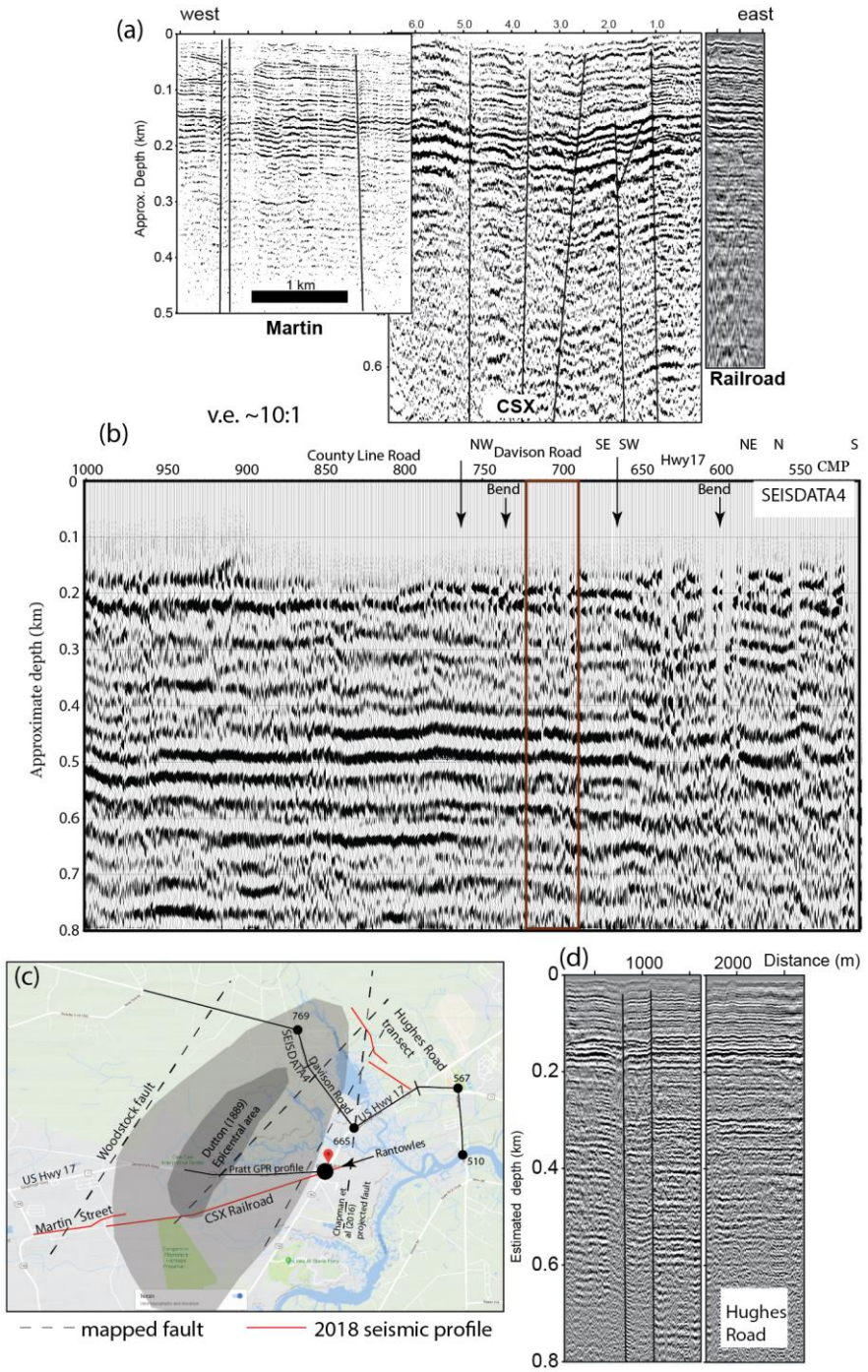

Figure 9. (a) Ravenel to Rantowles seismic transect consisting of Martin, CSX and Railroad Avenue profiles. Note the syncline and deformation zone along CSX profile and the Woodstock fault along Martin Street (b) Seisdata4 stack of Buckner, 2011 centered on the Davison Road portion of the profile. The brown box represents the along strike zone of deformation zone identified on the CSX and Hughes Road profiles. (c) map of profile locations and isoseismal zone of Dutton (1889). (d) Hughes Road profile showing a fault pair near the northern portion of the profile.

Data Archival

Seismic data are available immediately upon request from lliberty@boisestate.edu. Seismic field records will be archived at the Incorporated Research Institutions for Seismology (IRIS) as an assembled dataset (http://ds.iris.edu/ds/nodes/dmc/forms/assembled-id/). Archival will be submitted within one year of project completion (May 30, 2019).

References

Bakun, W. H., and Hopper, M. G. (2004). Magnitudes and locations of the 1811–1812 New Madrid Missouri and the 1886 Charleston, South Carolina, earthquake, *Bull. Seismol. Soc. Am*. 94, 64–75.

Bartholomew, M. J., and Rich, F. J. (2007). The walls of colonial Fort Dorchester: A record of structures caused by the August 31, 1886 Charleston, South Carolina earthquake and its subsequent earthquake history. Southeastern Geology, 44(4), 147-169.

Bollinger, G.A. (1977). Reinterpretation of the intensity data for the 1886 Charleston, South Carolina, earthquake, in Rankin, D.W., ed., Studies Related to the Charleston, South Carolina Earthquake of 1886: A Preliminary Report, *U.S. Geological Survey Professional Paper 1028*, p. 17-32.

Buckner, J. C. (2011). Crustal Structure in a Mesozoic Extensional Terrane: The South Georgia Rift and the Epicentral Area of the 1886 Charleston, South Carolina, Earthquake (Doctoral dissertation, Virginia Tech).

Chapman, M. C., and Beale, J. N. (2010). On the geologic structure at the epicenter of the 1886 Charleston, South Carolina, earthquake. Bulletin of the Seismological Society of America, 100(3), 1010-1030.

Chapman, M. C., Beale, J. N., Hardy, A. C., and Wu, Q. (2016). Modern Seismicity and the Fault Responsible for the 1886 Charleston, South Carolina, Earthquake. Bulletin of the Seismological Society of America, 106(2), 364-372.

Chapman, M. C., Martin, J. R., Olgun, C. G., & Beale, J. N. (2006). Site-response models for Charleston, South Carolina, and vicinity developed from shallow geotechnical investigations. Bulletin of the Seismological Society of America, 96(2), 467-489.

Coruh, C., J. K. Costain, J. C. Behrendt, and R. M. Hamilton (1981). New reflection seismic evidence for deformation of Mesozoic sediments near Charleston, S.C., Presented at the GSA Annual Meeting in Cincinnati, Ohio, GSA Abstract with Programs 13, no. 7, 13,431.

Dutton, C. E. (1889). The Charleston earthquake of August 31, 1886, in Ninth Annual Report of the U.S. Geological Survey to the Secretary of the Interior, J.W. Powell, Director, U.S. Geological Survey, Department of the Interior, U.S. Government Printing Office, Washington, D.C., 203–528.

Gribler, G., Liberty, L. M., Mikesell, T. D., & Michaels, P. (2016). Isolating retrograde and prograde Rayleigh-wave modes using a polarity mute. *Geophysics*, 81(5), V379-V385.

Hamilton, R. M., J. C. Behrendt, and H. D. Ackermann (1983). Land multichannel seismic-reflection evidence for tectonic features near Charleston, South Carolina, in Studies Related to the Charleston, South Carolina, Earthquake of 1886—Tectonics and Seismicity, G. S. Gohn (Editor), U.S. Geol. Surv. Profess. Pap. 1313, I1–I18.

Liberty, L.M., Hammer seismic reflection imaging in an urban environment, The Leading Edge, v. 30, no. 2, doi:10.1190/1.3555324, 2011.

Liberty, L.M. and Gribler, G., (2015). Shear wave seismic velocity profiling and depth to water

table/bedrock – earthquake site response measurements for Kootenai County, Idaho, Technical Report BSU CGISS 15-01, Idaho State Homeland Security Final Report, 76 p.

Marple, R. (2011). Comment on the Companion Articles "Finding Faults in the Charleston Area, South Carolina: 1. Seismological Data" by I. Durá-Gómez and P. Talwani and "Finding Faults in the Charleston Area, South Carolina: 2. Complementary Data" by P. Talwani and I. Durá-Gómez. *Seismological Research Letters,* 82(4), 599-605.

Marple, R. T., and R. Miller (2006). Association of the 1886 Charleston, South Carolina, earthquake and seismicity near Summerville with a 12° bend in the East Coast fault system and triple-fault junctions. Southeastern Geology 44 (3), 101–128.

Park, C.B., Miller, R.D., and Xia, J., 1999, Multichannel analysis of surface waves, *Geophysics*, 64, 800–808.

Schilt, F. S., L. D. Brown, J. E. Oliver, and S. Coffman (1983). Subsurface structure near Charleston, South Carolina: Results of COCORP reflection profiling in the Atlantic Coastal Plain, in Studies Related to the Charleston, South Carolina, Earthquake of 1886—Tectonics and Seismicity, G. S. Gohn (Editor), U.S. Geol. Surv. Profess. Pap. 1313, H1–H19.

Stephenson, W.J., Louie, J.N., Pullammanappallil, S., Williams, R.A., and Odum, J.K., 2005, Blind shear-wave velocity comparison of ReMi, and MASW results with boreholes to 200 m in the Santa Clara Valley: Implications for Earthquake Ground Motion Assessment, *Bulletin Seismological Society of America*, v. 95, n. 6, p. 2506-2516.

Talwani, P. (2011). Response to "Comment on the Companion Articles 'Finding Faults in the Charleston Area, South Carolina: 1. Seismological Data' by I. Durá-Gómez and P. Talwani andFinding Faults in the Charleston Area, South Carolina: 2. Complementary Data'by P. Talwani and I. Durá-Gómez" by R. Marple. *Seismological Research Letters*, 82(4), 606-608.

Talwani, P., and Durá-Gómez, I. (2009). Finding faults in the Charleston area, South Carolina: 2. Complementary data. *Seismological Research Letters*, 80(5), 901-919.

Talwani, P., and W. T. Schaeffer (2001). Recurrence rates of large earthquakes in the South Carolina Coastal Plain based on paleoliquefaction data, *J. Geophys. Res.* 106, no. B4, 6621–6642.

Van der Veen, M. and Green, A.G. (1998). Land streamer for shallow data acquisition: evaluation of gimbal-mounted geophones. Geophysics, 63, 1408-1413.

Weems, R.E., Lemon, E.M., Jr., Gohn, G.S., and Houser, B.B. (1987). Detailed sections from auger holes and outcrops in the Clubhouse Crossroads, Johns Island, Osborn, and Ravenel quadrangles, South Carolina: U.S. Geological Survey Open-File Report 87–661, 159 p. (available online at http://pubs.er.usgs.gov/publication/ofr87661.)

Weems, R. E., Lewis, W. C., & Lemon Jr, E. M. (2014). Surficial geologic map of the Charleston region, Berkeley, Charleston, Colleton, Dorchester, and Georgetown Counties, South Carolina (No. 2013-1030). US Geological Survey.

Wong, I., and 9 others, 2005, Potential losses in a repeat of the 1886 Charleston, South Carolina, Earthquake, Earthquake Spectra, v. 21, no 4, p. 1157-1184.